

A real-time velocity diagnostic for NSTX

M. Podestà and R. E. Bell

Princeton Plasma Physics Laboratory, Princeton, New Jersey 08543, USA

(Received 7 December 2011; accepted 19 February 2012; published online 12 March 2012)

A new system for fast measurements of the plasma toroidal velocity has been installed on the National Spherical Torus Experiment, NSTX [M. Ono *et al.*, Nucl. Fusion **40**, 557 (2000)]. The diagnostic, based on active charge-exchange recombination spectroscopy, can measure at up to six radial locations with maximum sampling rate of 5 kHz. The system is interfaced in real time with the NSTX plasma control system, in order to feed back on plasma velocity by means of actuators such as neutral beams and external coils. The paper describes the design criteria and implementation of the diagnostic. Examples from the initial tests of the system during neon glows are also discussed. © 2012 American Institute of Physics. [<http://dx.doi.org/10.1063/1.3692752>]

I. INTRODUCTION

Because of the profound effects of toroidal velocity, v_ϕ , on the stability and confinement properties of the plasma column,^{1,2} some degree of velocity control is highly desirable in tokamaks. Examples are provided by the JET,³ JT-60U,⁴ and DIII-D tokamaks,⁵ where v_ϕ data are made available in real time to the control system. This paper describes the real-time velocity (RTV) system that has been installed on the National Spherical Torus Experiment, NSTX,⁶ to measure the toroidal velocity, $v_\phi(R, t)$, with high temporal resolution. Information on v_ϕ is feed back to the NSTX plasma control system (PCS) (Ref. 7) for future implementation of real-time rotation control. NSTX (Fig. 1) is a spherical tokamak with major and minor radius $R_0 = 0.85$ m and $a \leq 0.65$ m. It produces deuterium and helium plasmas with a toroidal field ~ 5 kG and plasma current ~ 1 MA. Densities are $3 - 10 \times 10^{19} \text{ m}^{-3}$. Central electron and ion temperature are $T_e \approx T_i \sim 1$ keV. Neutral beam (NB) injection is the primary tool for heating and non-inductive current drive. The available power is $P_{NB} = 6$ MW, with injection energies of 60–90 keV for deuterium neutrals. Neutral beams are one of the two actuators available on NSTX for v_ϕ control. They mostly impart momentum to the bulk plasma, where the injected fast neutrals are deposited. The second actuator is a set of coils, commonly used for error field correction, that are capable of slowing down rotation through interaction with the edge plasma.⁸ Because NB and external coils act on different spatial regions, information on v_ϕ from both the core and the edge regions is required to implement velocity control.

Active charge-exchange recombination spectroscopy (CHERS) is routinely used on NSTX for off-line determination of plasma rotation.⁹ The main CHERS system consists of a fixed-wavelength spectrometer¹⁰ coupled to a CCD detector with fixed sampling rate of 100 Hz. Density, temperature, and toroidal rotation of carbon impurity ions are inferred from intensity, broadening, and wavelength Doppler shift of the C VI line at $\approx 5291 \text{ \AA}$ ($n = 8-7$ transition). Two sets of views are used to separate the charge-exchange (*active*) C VI emission that originates in the region intercepting the NB from the background (*passive*) contribution (Fig. 1). The latter set is toroidally displaced with respect to the NB volume.

Except for cases when the axi-symmetry is lost, e.g., during plasma disruptions, the use of displaced views provides accurate background measurements without the need of modulating one or more NB sources, which can then be used for control purposes. Measurements and parameters of the CHERS diagnostic were used as a reference to design the RTV system.

II. RTV DESIGN CRITERIA AND IMPLEMENTATION

The main requirement for the RTV system is a high sampling rate at which plasma velocity data are analyzed and made available to the NSTX PCS for implementation of real-time rotation control. Based on CHERS measurements, v_ϕ typically evolves on time scales ~ 10 ms, whereas NB and external coils affect the plasma on time scales $\sim 10-50$ ms. Consequently, the minimum requirement from PCS was defined as 1 frame every 3 ms (frame rate ~ 330 Hz). The target sampling rate for the RTV system was set to ~ 1 kHz, which is reasonably faster than the v_ϕ time scales to implement flexible control schemes. To meet this target, the amount of light collected by RTV needs to be increased with respect to CHERS. For instance, neglecting the different sensitivity of the two systems, RTV at a frame rate of 1 kHz has to collect a photon flux 10 times larger than CHERS at 100 Hz to match the CHERS uncertainty in velocity of $\sim 0.5\%$. Moreover, a real-time analysis algorithm of the measured spectra that minimizes the computing time needed to be developed, see Sec. III. Table I compares the main parameters of CHERS and RTV. The design criteria and the components of the RTV system are described in more detail here below.

A. General layout

The signal is collected from the plasma through optics with f -number $f/1.8$ (background views) and $f/3.4$ (active views). The latter optics are shared with the NSTX motional Stark effect system.¹¹ Light is then transported to a separate diagnostic room, where the spectrometers are located, by means of optical fibers¹² (approximate length is 35 m). This allows access to the diagnostics during NSTX operations

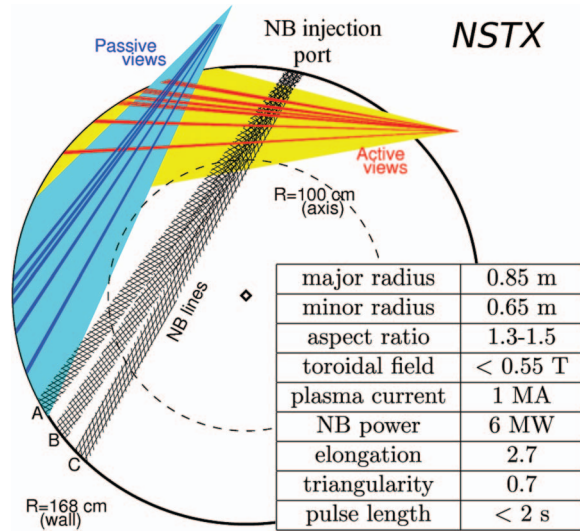


FIG. 1. Top view of NSTX with a layout of the RTV active and background midplane sightlines (thick lines) with respect to the NB lines (A, B, and C). The magnetic axis is at $R \approx 100$ cm. The shaded regions indicate the region of measurements of the CHERS systems. The table summarizes the main NSTX parameters.

and minimizes the noise induced on the detectors by neutrons and gammas from the plasma. A SMA-to-SMA patch-panel (where SMA indicates the Sub-Miniature version A connector type) in the diagnostic room is used to terminate available spare CHERS fibers from the toroidal system along with newly installed background fibers. It is also used to select the configuration of active/background channels. For instance, 4 pairs of active and background channels are measured in the standard configuration, with each channel measured through 8 fibers focused at the same radial location (see below). If the signal strength is large enough, up to 6 active channels can be measured by reducing the number of fibers used for each channel.

B. Number and location of sightlines

The number of radial channels has been chosen as a compromise between two requirements, i.e. (i) to minimize the number of sightlines to reduce the complexity of the system, and (ii) to provide sufficient information on the evolution of $v_\phi(R, t)$ for physics studies and feedback control. A first constraint on the location of the RTV views comes from the fact that spare CHERS sightlines are used for the active RTV signals, thus limiting the choice of available locations. Based on the number of available actuators, at least 2 measurements are

TABLE I. Main parameters of the CHERS and RTV systems. Values in parenthesis refer to the background views.

System	CHERS	RTV
No. of channels	51 (39)	6 (5)
Fiber diameter (μm)	210 (600)	210 (210)
Fibers/channel	2 (1)	8 (7)
Frame rate	100 Hz	≤ 5 kHz
Measured quantities	v_ϕ, n_C, T_C	v_ϕ
Monitored line	C VI, 5291 Å	

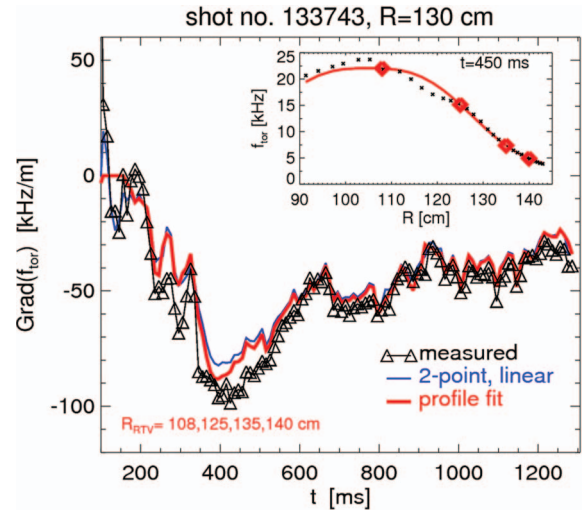


FIG. 2. Example of the radial gradient of the toroidal rotation frequency at $R = 130$ cm measured by CHERS (triangles). Lines show the gradient reconstructed through a fit of the radial profile (thick line) and by a two-points linear interpolation (thin line) based on the simulated RTV data. The inset shows a rotation profile from CHERS (dots) and a fit with a modified gaussian based on four measurements points (diamonds) to mimic RTV measurements.

required where actuators are more effective, i.e., in the core (NB) and at the edge (external coils). Additional channels are desirable to provide estimates of the local v_ϕ gradient. The rotation profile measured by CHERS has been used to further optimize the number and radial location of the sightlines. The optimization is based on the observation that the toroidal rotation profile, $f_{tor}(R) = v_\phi(R)/2\pi R$, can be modeled reasonably well on NSTX by fitting the radial profile with a modified gaussian function,

$$f_{tor}(R) \approx f_0 \times \exp^{-\log(2) \left[4 \frac{(R-R_c)^2}{\Delta R^2} \right]^s} + \Delta f. \quad (1)$$

In principle, this function has 5 free parameters: amplitude f_0 , center radius R_c , full width at half maximum (FWHM) ΔR , and offset Δf . A fifth parameter, s , determines the *squareness* of the profile. s varies from $s < 1$ (triangular shapes) to $s > 1$ (square shapes), with $s = 1$ for a gaussian curve. In practice, the center radius equals the magnetic axis and does not vary substantially during a discharge. The offset can also be approximated by the value of f_{tor} close to the separatrix, at $R \approx 140-145$ cm. The number of free parameters in the fit is therefore reduced to 3, which sets the minimum number of required channels. Tests with $n_{ch} = 3 \dots 6$ have been done, using the error in the reconstructed $f_{tor}(R, t)$ and its radial gradient (and the increased cost and complexity for increasing number of channels) as metric to define the optimum n_{ch} . It results that $n_{ch} = 4$ provides a sufficiently accurate reconstruction of $f_{tor}(R, t)$, hence of $v_\phi(R, t)$ (Fig. 2). The nominal locations are $R = 108, 125, 135, 140$ cm (see inset in Fig. 2), with spare views at $R = 130, 145$ cm.

C. Number and size of fibers

The target design required that RTV at frame rate of ~ 1 kHz had a similar signal-to-noise ratio (SNR) as CHERS at 100 Hz, with uncertainties $\lesssim 0.5\%$ for operations with

two NB sources at full power (4 MW total). For the active channels, obtained from pre-existing spare CHERS views, the fiber's core diameter is $210\ \mu\text{m}$. The condition on the SNR leads to 8 fibers per channel. The small fiber size, along with the relaxed requirements in accuracy for temperature measurements with respect to CHERS, implies that the spectrometers can operate without an input slit and thus increase the number of photons collected. Because of the resulting instrumental width, only ion temperatures $\gtrsim 300\ \text{eV}$ can be inferred. For the passive views, 5 new channels have been installed. Each channel is composed by a bundle of 7 fibers with diameter of $210\ \mu\text{m}$. Bundles are packed in circular ferrules on the machine side to match the radial spread of the active channels, taking into account the differing magnification between active and passive lenses.

D. Spectrometer

The RTV system utilizes Holospec spectrometers from Kaiser Optical Systems.¹³ Short sections ($\sim 7\ \text{m}$) of fibers from the patch panel are collected on a fiber holder (Fig. 3) that attaches to the spectrometer input. Fibers are arranged on the holder in 2 horizontally displaced, curved columns (see inset in Fig. 3). The curvature is optimized to obtain straight vertical images on the CCD plane,¹⁰ which minimizes the instrumental width when the CCD is binned. The 2 columns result in 2 spectra accommodated on the same row on the CCD.

Light enters the spectrometer through a $85\ \text{mm}$, $f/1.8$ input lens which collimates the light into a parallel beam. A band-pass filter¹⁴ selects the wavelength range of interest, see below. The light is diffracted by the grating and collected on a $50\ \text{mm}$, $f/1.2$ output lens. A ratio of focal lengths of $85/50 = 1.7$ is chosen to de-magnify the image at the output of the spectrometer and match the CCD size. The use of a chopper between the output lens and the detector was omitted to allow more flexible timing. The spectrometer and CCD detector are mounted on a six-axis stage to align the system and achieve an optimal focus across the detector.

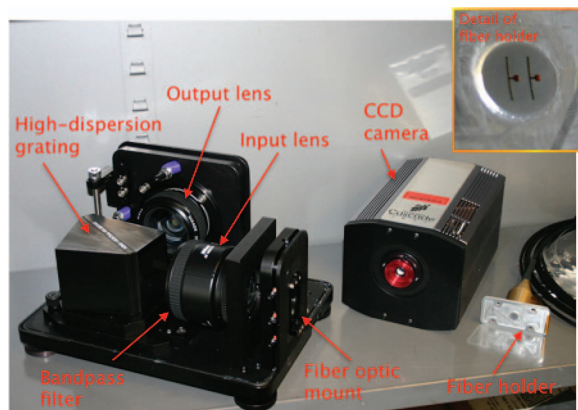


FIG. 3. Main components of the RTV spectrometers. Fibers from NSTX are arranged in two columns on a curved-slit fiber holder, see inset, attached to the spectrometer. Light focused in a parallel beam by the $f/1.8$ input lens is filtered around the C VI line of interest, diffracted by the grating and re-focused on a CCD detector by the output $f/1.2$ lens.

E. Wavelength range and grating

Toroidal velocities on NSTX are in the range (-120 , $+350$) km/s, which corresponds to a Doppler shift of the observed C VI line of (-2.1 , 6.2) Å. The wavelength range for RTV was defined to be $\approx 5284\text{--}5309\ \text{Å}$, to measure both the C VI emission line at $5290.5\ \text{Å}$ and the Ne I lines at $5298.19\ \text{Å}$ and $5304.756\ \text{Å}$ (Ref. 15) (see Sec. IV), that are used for the wavelength calibration of the instruments. These specifications are met by a *high-dispersion transmission grating*¹³ with custom center wavelength of $5297\ \text{Å}$.

F. Frame rate, CCD detector

The required frame rate for implementation of v_ϕ control was $\sim 330\ \text{Hz}$. Apart from control, higher rates are desirable to discern transient effects related, for instance, to change in plasma confinement mode (L-H transition) or to MHD phenomena. The target frame rate, along with a required 16-bit dynamic range, restricted the choice among available CCD detectors. The Cascade 128+ camera¹⁶ was finally chosen, although its CCD size of $\approx 3 \times 3\ \text{mm}$ requires splitting the 4 pairs of channels across 2 cameras. The maximum frame rate achievable with vertical binning of the CCD is 5 kHz.

Based on the number and size of fibers and on the choice of grating and CCD detector, the arrangement of the spectra on the CCD has been defined, see Fig. 4. The CCD is partitioned into 4 horizontal strips (*bins*), with the signal for each channel split over 2 bins. Each bin contains 2 spectra in the horizontal direction. Pixels from the same bin are added together in the vertical direction to improve the SNR and reduce the read-out time. No horizontal binning is used.

Because the camera is operated with neither a chopper nor an built-in shutter, smearing of the spectra during the frame shift can occur. To minimize the effects of smearing, background bins with reduced signal are read out before the

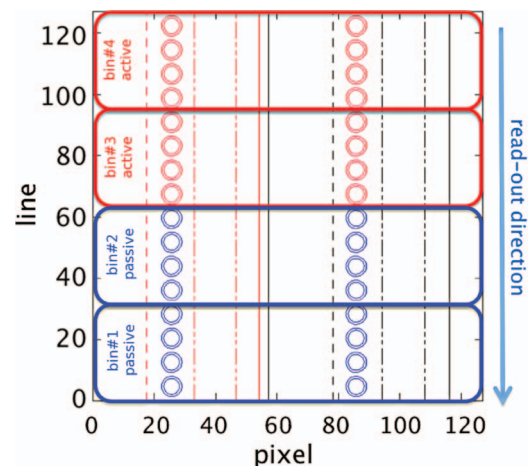


FIG. 4. Layout of the fiber's arrangement on the CCD detector. Circles show the equivalent fiber size on the CCD. Only 7 of the 8 available fibers are actually used for the background views. Vertical dashed lines are the expected positions of C VI (dashed) and Ne I (dotted-dashed) lines. Vertical solid lines delimit the pixel range corresponding to the wavelength range of the bandpass filter. Two spectra are accommodated on each row of the detector. A typical vertical binning strategy with 4 vertical bins is illustrated by the rectangular regions.

brighter active bins. Residual effects of smearing will appear as a frame-rate-dependent enhancement of the background light in the active spectra, which can be compensated via software during the analysis.

III. DIAGNOSTIC CONTROL AND REAL-TIME ANALYSIS

A control and analysis algorithm has been implemented in the C++ language. The use of this relatively low-level language reduces over-head PC operations and improves the efficiency and reliability of the system. The software serves 3 main functions, namely (i) diagnostic control and data acquisition, (ii) data analysis, and (iii) communication with PCS. Each part is discussed below in detail.

A. Control and data acquisition

Each CCD camera is controlled by a multi-processor computer. For the initial tests, a Windows[®] operating system was used. The latter will be converted to a Unix-based system for better integration with PCS and to improve stability and performance of the control and analysis code. The main settings of the system, such as exposure time and duration of the acquisition, can be adjusted before a plasma discharge through an IDL-based graphical user interface.¹⁷ Synchronization with other NSTX sub-systems is performed by means of MDSplus *events*,¹⁸ indicating at which point of the sequence the control PC should perform pre-defined actions such as arming the CCD cameras, waiting for a trigger and downloading data after the sequence has completed. The cameras receive a trigger for each frame from a waveform generator, which can be programmed to deliver variable frame rates within the same discharge to efficiently exploit the dynamic range of the instrument. For example, the frame rate could be reduced during phases with low signal, or increased when saturation of the CCD is detected. Two schemes can be used to optimize the frame rate during a discharge, based on (i) a pre-programmed waveform for the frame rate (e.g., based on the NB waveform), or (ii) feed-back on the frame rate via the control software. For the latter option, the response time of the waveform generator to adapt the frame rate is ≈ 150 ms. The initial trigger for the generator is provided by the NSTX clock, controlled by a EPICS system.¹⁹ Once the discharge has terminated, data are uploaded to the MDSplus database for subsequent, off-line analysis.

B. Real-time data analysis

The real-time analysis is performed after each exposure. Raw data are first corrected for a pre-defined calibration curve for each bin (channel). Data from each active/background pair are re-sampled on a common wavelength basis. A least-square fit of the resulting spectrum, which contains both background-only and background plus active components, is then performed. The spectrum is modeled as two distinct gaussian peaks, representing the background and active (charge-exchange only) emission. Free parameters are inten-

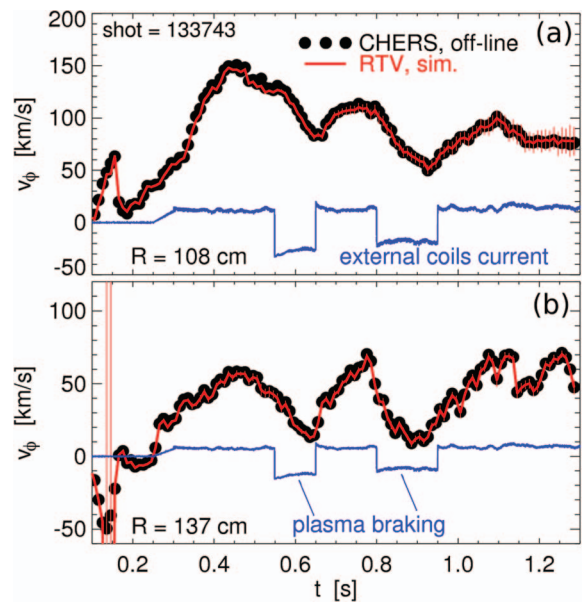


FIG. 5. Toroidal velocity calculated through the standard, post-shot CHERS analysis (symbols) and through the RTV analysis software (line). The same CHERS data from (a) the core and (b) the edge are used for both analyses. Negative pulses of coils current (shown in arbitrary units) correspond to phases of magnetic braking, which results in a decrease of v_ϕ over time scales of 10's of milliseconds.

sity of active and background lines, their fullwidth at half maximum and the center wavelength of the peaks. The wavelength shift of the active peak is finally converted into the corresponding velocity, which represents the input quantity for PCS.

A comparison between the standard off-line analysis of plasma velocity from CHERS data and the results of the RTV fitting code is shown in Fig. 5. For this particular discharge, the external coils were used at two different times to slow down plasma rotation. In spite of its simplified algorithm with respect to the off-line analysis, the RTV fitting software reproduces very well the $v_\phi(t)$ evolution. Further optimization of the fit algorithm will be considered after the initial RTV operations with NB-heated NSTX plasmas. Possible improvements are (i) including information on the instrumental function to model the peaks, (ii) modeling deviations of the active peak from a gaussian shape for large toroidal velocities, and (iii) accounting for the possible contamination of the background spectrum by *plume* emission.²⁰

The fit algorithm is based on the Levenberg-Marquardt method, implemented in an open-source C++ library.²¹ The algorithm has been optimized for *distributed* operations through the OpenMP[®] set of libraries.²² Each of the 4 processors can execute 2 processes. The total computing time for up to 8 channels is $\lesssim 120 \mu\text{s}$. After the fit, velocity data for each channel are sent to a digital-to-analog converter which translates the digital results into an analog signal, made available to PCS (see below). An upgrade of this implementation, based on the presently available PCS hardware, with a fully digital data transfer scheme is under consideration. The minimum latency in the communication with PCS is $100 \mu\text{s}$, which is the inherent delay between frame exposure and end of read out.

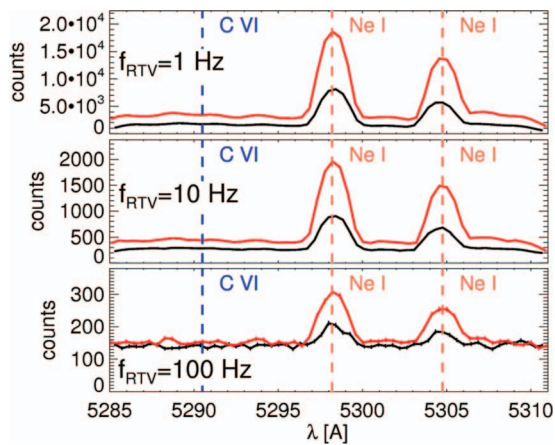


FIG. 6. Neon spectrum measured by two adjacent channels during a neon glow on NSTX for different RTV frame rates. Vertical lines indicate the rest wavelength of the Ne I lines that dominate the spectrum and of the expected C VI line. Because the light during glows is $\gtrsim 50$ times dimmer than for typical NSTX plasmas, frame rates quoted in the panels are qualitatively representative of 50 500 and 5000 Hz frame rates during experiments in terms of counts on the detector.

At this point, the system is ready for the next frame and the cycle repeats until the required number of frames is acquired.

C. Communication with PCS

For the initial tests of RTV, the analyzed velocity data and the associated uncertainties are spooled out to a digital-to-analog PCI card²³ connected to PCS. Each card has four analog output channels with 16 bit resolution. The analog output is read by PCS every 200 μ s and converted back into digital format to process the information on toroidal velocity. Based on the RTV input, a control scheme can be implemented on PCS to control rotation by means of the available actuators.

IV. EXAMPLES FROM NEON GLOW DISCHARGES

Examples of spectra measured by RTV during a neon glow discharge²⁴ are shown in Fig. 6. The two dominant lines are Ne I lines at 5298.19 Å and 5304.756 Å. Other lines, probably originating from molecular emission, are visible just above the background level. The Ne I lines are used as reference to calculate the wavelength calibration of the instrument. The resulting dispersion is ≈ 0.43 Å/pixel. The full width at half maximum is ≈ 4 pixels, or ≈ 300 eV in terms of energy, consistently with the design value. Wavelength calibration from neon glows is preferred to calibration with neon lamps because it ensures the same illumination of the system as during actual experiments.

The RTV and CHERS spectra are compared in Fig. 7. CHERS is run at its nominal frame rate for plasma operations of 100 Hz. Because the light level during the glow is $\gtrsim 50$ times dimmer than for typical NSTX plasmas, CHERS calibration data are noisy. (Note that acquisitions for calibration purposes during Ne glow typically have exposure times of several minutes). To improve the comparison, CHERS spectra are summed over 10 frames via software, thus bringing the effective frame rate from 100 Hz to 10 Hz. The com-

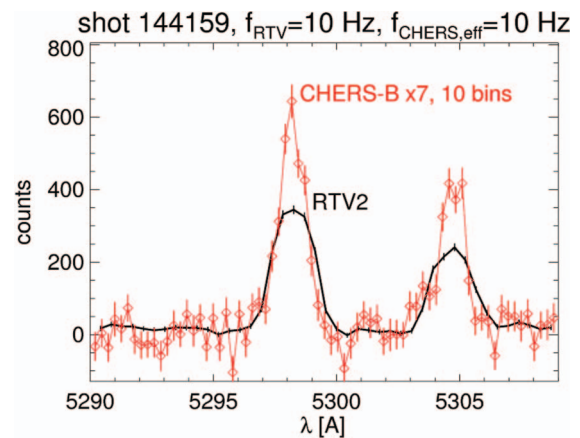


FIG. 7. Comparison of RTV (line) and CHERS (diamonds) spectral data from a Ne glow discharge from sightlines with tangency radius of 108 cm (close to the vacuum chamber center). RTV frame rate is 10 Hz. For CHERS, 10 frames are added together to reach an effective rate of 10 Hz.

parison confirms that the RTV system collects much more light than CHERS, by virtue of the increased number of fibers per channel (4 in the example shown in Fig. 7), the absence of chopper and entrance slit on the spectrometer and the improved transmission of the bandpass filter and grating of the RTV systems. The improved quality of the RTV data can be quantified by the small uncertainties in the Ne I rest wavelength inferred from a fit of the Ne peaks (Fig. 8) for multiple frames. For neon glow data, the standard deviation over 100 frames is ± 0.012 Å for the RTV spectra, that corresponds to ± 0.7 km/s. For comparison, a fit of the CHERS data gives a standard deviation of ± 0.05 Å.

In conclusion, a new system for fast measurements of the plasma toroidal velocity has been implemented on NSTX. Depending on the photon flux from the plasma, the velocity can be measured at 4–6 radial locations at frame rates ≤ 5 kHz. Uncertainties are anticipated to be $\ll 5\%$. A dedicated software for real-time analysis of the spectra has been developed. Values of velocity from such analysis are transmitted in real time to the NSTX PCS, which will permit the implementation of a feedback control on plasma rotation by means of neutral beams and external coils. Initial tests from neon glow discharges confirm that the design parameters have been met or exceeded. The first operation of the RTV system is planned after the upgrade of the NSTX device is completed.

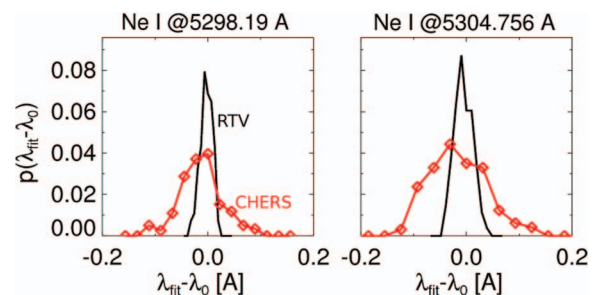


FIG. 8. Distribution $p(\lambda_{fit} - \lambda_0)$ of the spread of Ne I rest wavelength inferred from a fit of Ne I lines, λ_{fit} , with respect to the nominal Ne I rest wavelength, λ_0 . Data refer to 100 spectra measured by RTV (line) and CHERS (diamonds) under the same conditions as in Fig. 7. The narrower distribution from RTV data indicates a smaller uncertainty in the inferred wavelength.

ACKNOWLEDGMENTS

The authors would like to thank R. E. Feder, J. M. Carson, and C. B. McLaughlin for their help in the design and implementation of the RTV system. Discussions with Dr. S. A. Sabbagh (Columbia University, NY - USA) and with the NSTX Control Group are gratefully acknowledged. Work supported by U.S. Department of Energy (DOE) (Contract No. DE-AC02-09CH11466).

¹J. W. Berkery, S. A. Sabbagh, R. Betti, B. Hu, R. E. Bell, S. P. Gerhardt, J. Manickam, and K. Tritz, *Phys. Rev. Lett.* **104**, 035003 (2009).

²P. W. Terry, *Rev. Mod. Phys.* **72**, 109 (2000).

³P. J. L. Heesterman, I. Sall, C. Giraud, K.-D. Zastrow, A. Meigs, R. Felton, and E. Joffrin, *Rev. Sci. Instrum.* **74**, 1783 (2003).

⁴M. Yoshida, Y. Sakamoto, M. Sueoka, Y. Kawamata, N. Oyama, T. Suzuki, Y. Kamada, and the JT-60 Team, *Fusion Eng. Des.* **84**, 2206 (2009).

⁵J. T. Scoville, D. A. Humphreys, J. R. Ferron, and P. Gohil, *Fusion Eng. Des.* **82**, 1045 (2007).

⁶M. Ono, S. M. Kaye, Y.-K. M. Peng, G. Barnes, W. Blanchard, M. D. Carter, J. Chrzanowski, L. Dudek, R. Ewig, D. Gates, R. E. Hatcher, T. Jarboe, S. C. Jardin, D. Johnson, R. Kaita, M. Kalish, C. E. Kessel, H. Kugel, R. Maingi, R. Majeski, J. Manickam, B. McCormack, J. Menard, D. Mueller, B. Nelson, B. Nelson, C. Neumeyer, G. Oliaro, F. Paoletti, R. Parsells, E. Perry, N. Pomphrey, S. Ramakrishnan, R. Raman, G. Rewoldt, J. Robinson, A. L. Roquemore, P. Ryan, S. Sabbagh, D. Swain, E. J. Synakowski, M. Viola, M. Williams, J. R. Wilson, and NSTX Team, *Nucl. Fusion* **40**, 557 (2000).

⁷D. Mastrovito, D. Gates, S. P. Gerhard, J. Lawson, C. Ludescher-Furth, and R. Marsala, *Fusion Eng. Des.* **85**, 447 (2010).

⁸W. Zhu, S. A. Sabbagh, R. E. Bell, J. M. Bialek, M. G. Bell, B. P. LeBlanc, S. M. Kaye, F. M. Levinton, J. E. Menard, K. C. Shaing, A. C. Sontag, and H. Yuh, *Phys. Rev. Lett.* **96**, 225002 (2006).

⁹R. E. Bell, R. Andre, S. M. Kaye, R. A. Kolesnikov, B. P. LeBlanc, G. Rewoldt, W. X. Wang, and S. A. Sabbagh, *Phys. Plasmas* **17**, 082507 (2010).

¹⁰R. E. Bell, *Rev. Sci. Instrum.* **75**, 4158 (2004).

¹¹F. M. Levinton and H. Yuh, *Rev. Sci. Instrum.* **79**, 10F522 (2008).

¹²See www.fiberguide.com for Fiberguide Industries, Inc.

¹³See www.kosi.com for Kaiser Optical Systems, Inc.

¹⁴Williams Advanced Materials, BARR Precision Optics.

¹⁵Wavelengths of spectral lines from the Atomic Line List database at <http://www.pa.uky.edu/~peter/atomic/index.html>.

¹⁶The main specifications of the Cascade 128+ camera can be found at <http://www.photometrics.com/>.

¹⁷See <http://ittvis.com/> for more information on the IDL language.

¹⁸See <http://www.mdsplus.org/> for more information on the MDSplus data acquisition software.

¹⁹D. Mastrovito, W. Davis, J. Dong, P. Roney, and P. Sichta, *Fusion Eng. Des.* **81**, 1847 (2006).

²⁰R. E. Bell, *Rev. Sci. Instrum.* **77**, 10E902 (2006).

²¹Documentation for the LEVMAR suite of routines by M. I. A. Lourakis can be found at <http://www.ics.forth.gr/~lourakis/levmar/>.

²²See <http://openmp.org/> for details on the OpenMP project.

²³National Instruments PCIe-6259M.

²⁴Glow discharges are used on NSTX for two purposes: cleaning (or *conditioning*) of the plasma facing components, using helium, or wavelength calibration of optical systems, using neon.